Catalysis Communications 40 (2013) 139–144

Contents lists available at SciVerse ScienceDirect

Catalysis Communications

journal homepage: www.elsevier.com/locate/catcom

Short Communication

Synthesis, characterization and catalytic application of Au NPs-reduced graphene oxide composites material: an eco-friendly approach

Ponchami Sharma [a], Gitashree Darabdhara [a], Tallapareddy Muralikrishna Reddy [a], Ashwini Borah [a], Pranjal Bezboruah [b], Pranjal Gogoi [b,*], Najrul Hussain [a], Pinaki Sengupta [a], Manash R. Das [a,*]

[a] Materials Science Division, CSIR-North East Institute of Science and Technology, Jorhat-785006, Assam, India
[b] Medicinal Chemistry Division, CSIR-North East Institute of Science and Technology, Jorhat-785006, Assam, India

ARTICLE INFO

Article history:
Received 25 April 2013
Received in revised form 16 June 2013
Accepted 18 June 2013
Available online 22 June 2013

Keywords:
Graphene oxide
Gold nanoparticle
Ascorbic acid
Aerobic oxidation

ABSTRACT

In this paper, we have reported the synthesis of Au NPs-reduced graphene oxide (rGO) composites under microwave irradiation using ascorbic acid as eco-friendly reducing agent. The formation of Au NPs-rGO composites was confirmed by UV/Visible spectroscopy, DRIFT spectroscopy, TGA, XRD analysis, SAXS and HRTEM. HRTEM analysis results show that the particle size of the Au NPs formed on rGO nanosheets were in the range of 2-20 nm which is also supported by SAXS analysis results. The synthesized Au NPs-rGO composites were successfully utilized for the aerobic oxidation of benzyl alcohols to their corresponding aldehydes.

1. Introduction

Graphene, the single-layered two-dimensional allotrope of carbon, has created a new renaissance in the field of nanoscience and nanotechnology [1,2]. The closely packed honeycomb of sp^2 hybridized carbon network enriches graphene with extraordinary electrical, thermal and mechanical properties [3–9]. Graphene-based materials modified with metal nanoparticles (NPs) have in particular got interest for the development of advanced materials for a number of applications. However, the individual graphene sheets have a tendency to restack to form layered graphite structure due to strong van der Waals interaction. Insertion of the metal NPs into the graphene sheets is proved to be very effective in preventing such restoring. In view of this recent research, efforts have focused on the synthesis of metal NPs-graphene oxide (GO)/graphene composite materials [10]. Metallic NPs are important in different area such as catalysis, microelectronics, light emitting diodes, photovoltaic cells, surface-enhanced Raman scattering (SERS) or localized surface plasmon resonance (LSPR) and also in medical or biological applications [11]. Moreover, metal NPs show changes in their electronic, optical and catalytic properties, depending on the method of synthesis [12]. Thus, insertion of metal NPs onto graphene-based matrix represents an important study for the exploration of their properties and applications.

A number of methods have been reported for synthesis of metal NPs-graphene composites. Among them solution chemistry approach [13–17], electrochemical deposition of metal NPs onto graphene sheets [18], ultrasonication [19], microwave irradiation [20], etc., are most widely used. Typically, most of the method involves the simultaneous reduction of the metal salt and GO nanosheets [13–17]. $NaBH_4$ and hydrazine hydrate are most widely used reducing agent for the synthesis of the metal NPs-GO/reduced graphene oxide (rGO) composite materials. However, toxicity is the major disadvantage of these two reagents. Nowadays, searching for an efficient, less toxic, eco-friendly reducing agent is of great significance for the preparation metal NPs-GO/rGO composite materials. Ascorbic acid is an environment friendly reducing agent, which is widely used in redox reactions. The excess acid can be easily removed from the reaction mixture by decomposition using H_2O_2.

The oxidation of benzyl alcohol is an important reaction for the production of benzaldehyde, which is widely used in perfumes, pharmaceuticals, dyestuffs, agrochemicals and as plastic additives [21]. Benzaldehyde can be obtained by many processes as liquid phase chlorination and oxidation of toluene, partial oxidation of benzyl alcohol, alkali hydrolysis of benzal chloride and the carbonylation of benzene. However, most of the process provides benzaldehyde with trace contamination from chlorine, which is not suitable in perfumes and pharmaceuticals. On the other hand, in the catalytic vapor-phase oxidation of benzyl alcohol to benzaldehyde [22], a very significant carbon loss in the form of carbon oxides is a major problem. A few processes have been reported for the liquid phase oxidation of benzyl alcohol to benzaldehyde over Pd [23], heteropoly acid [24] and

---

* Corresponding authors. Fax: +91 376 2370011.
E-mail addresses: gogoipranj@yahoo.co.uk (P. Gogoi), mnshrdas@yahoo.com (M.R. Das).

1566-7367/$ – see front matter © 2013 Elsevier B.V. All rights reserved.
http://dx.doi.org/10.1016/j.catcom.2013.06.021

Ni-Al-hydrotalcite [25], using molecular oxygen or aqueous H_2O_2 as terminal oxidant. Recently, Au NPs is considered as the catalyst of choice for the oxidation of benzyl alcohol [26–32]. Although these methods often show excellent activity, many of these are associated with several shortcomings such as low yield, use of organic solvent, transition-metal, etc., there is a need to develop a convenient and more active catalyst for the benign oxidation of benzyl alcohol. In this paper, we report the catalytic application of Au NPs-rGO for the oxidation of benzyl alcohol to benzaldehyde under organic-solvent-free condition, where O_2 is used as an oxidant (Scheme 1). The Au NPs-rGO composites were synthesized using eco-friendly ascorbic acid as a reducing agent under microwave irradiation which avoids the use of toxic reducing agents such as $NaBH_4$, hydrazine hydrate, etc.

2. Experimental

2.1. Preparation and characterization of GO nanosheets

GO nanosheet was synthesized from powder graphite adopting the Hummer and Offeman [33] method. A detailed synthesis method of GO nanosheets is discussed in previously published paper [14].

2.2. Preparation of Au NPs-rGO composites and rGO nanosheets

The Au NPs-rGO composites material was synthesized by using environment friendly, nontoxic reducing agent, ascorbic acid under microwave irradiation. The detailed experimental procedure for synthesis of Au NPs-rGO composites material is described in supporting information. Synthesis of rGO was also carried out adopting the same procedure without adding Au-salt to have better understanding of reduction of GO nanosheets during the formation of Au NPs-rGO composites.

2.3. Catalytic experiments

The liquid phase oxidation was carried out in an ACE pressure tube filled with oxygen. Water suspension of Au NPs-rGO composites (8.1 mg in 2 mL), benzyl alcohol (1 mmol) and K_2CO_3 (3 mmol) were placed in a glass ACE pressure tube (10 mL) with a magnetic stirrer bar. The tube was sealed with a rubber O-ring and threaded Teflon seal under O_2, and the entire mixture was vigorously stirred at 130 °C (bath temperature) for 4 h. The reaction mixture was cooled to room temperature and the organic product was extracted with ethyl acetate (3 × 10 mL). The aqueous phase was separated and could be used consecutively for another three times for the oxidation of benzyl alcohols (1st recycle 73%, 2nd recycle 74% and 3rd recycle 70% benzaldehyde was obtained). The upper organic phase was dried and concentrated under reduced pressure. The product was purified by column chromatography.

3. Results and discussion

3.1. Characterization of GO nanosheets

The complete characterization of the synthesized GO nanosheets from graphite powder was reported in the previously published paper [14].

3.2. Characterization of AuNP-rGO composites and rGO nanosheets

3.2.1. UV/Visible spectroscopy

The formation of Au NPs on the rGO nanosheets by microwave irradiation using ascorbic acid as reducing agent was primarily monitored by UV/Visible spectroscopy as shown in Fig. 1. GO nanosheets shows two characteristic peaks at 241 nm and 308 nm due to $\pi \rightarrow \pi^*$ and $n \rightarrow \pi^*$ transitions, respectively. The $n \rightarrow \pi^*$ peak disappears upon reduction of GO to rGO. Similar observation was also obtained in the UV/Visible spectra of AuNPs-rGO composites. The appearance of a characteristic surface plasmon resonance (SPR) band at 545 nm indicates the formation of Au NPs on the rGO nanosheets.

3.2.2. Thermogravimetric analysis

The simultaneous conversion of GO to rGO nanosheets by ascorbic acid with the formation of Au NPs is reflected in the thermogravimetric (TGA) curves. It is observed from the Fig. 2 that the thermal stability of GO nanosheet is much lower than the raw graphite. The main weight loss takes place around 200 °C (37.72%) due to pyrolysis of the labile oxygen-containing functional groups [13]. The weight loss in this region decreases up to 17.17% upon formation of Au NPs-rGO composites due to the reduction of these oxygen containing functional groups. Moreover, the weight loss associated with high temperature pyrolysis of Au NPs-rGO composites above 600 °C is similar to that for graphite and rGO, which results from pyrolysis of the carbon skeleton of rGO nanosheets [13].

3.2.3. X-ray diffraction analysis

The formation of the Au NPs on rGO nanosheets is further characterized by X-ray diffraction (XRD) analysis as shown in Fig. 3. The XRD pattern of GO shows a characteristic peak at 2θ value of 11.72. The intensity of this peak considerably decreases upon formation of rGO, and two new peaks appear at 2θ value of 23.82 and 42.62. Similar observation was also found in the XRD pattern of Au NPs-rGO composites. Moreover, the prominent peaks in the XRD pattern of at 2θ values of about 38.08°, 44.34°, 64.50°, 77.48° and 81.68° corresponding to d-spacing of the Au NPs are 2.36, 2.04, 1.44, 1.23 and 1.18 Å are assigned to the (111), (200), (220), (311) and (222) crystallographic planes of cubic Au NPs, respectively (JCPDS card No 004-0784). The high intense diffraction peak observed at 38.08°, corresponding to the crystalline Au, confirms that the NPs are composed of pure crystalline Au. The crystallite size of the Au NPs is calculated

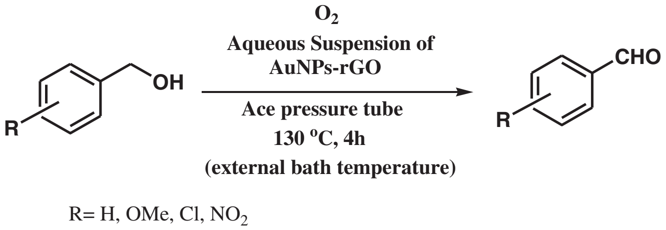

Scheme 1. Au NPs-rGO-catalyzed aerobic oxidation of benzyl alcohol.

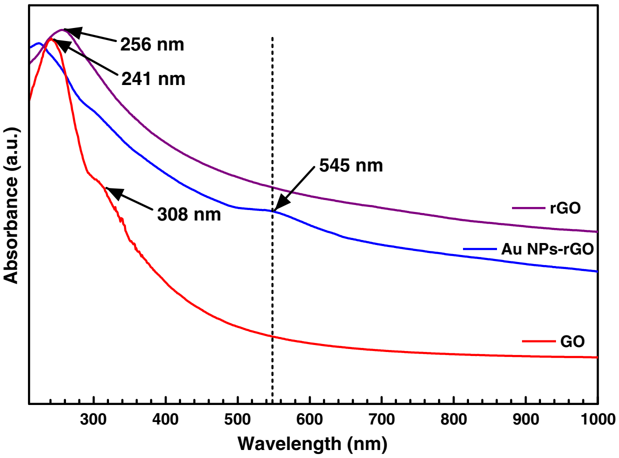

Fig. 1. UV/visible spectra of GO, rGO and Au NPs-rGO composites in water.

by Sherrer equation using PDXL software and found to be ~20 nm, which is also supported the TEM analysis results.

3.2.4. Small-angle X-ray scattering analysis

Small-angle X-ray scattering (SAXS) is another technique used to understand the particle size distribution of the Au NPs on the rGO nanosheets. The SAXS intensities of the Au NPs on rGO were plotted as a function of the scattering vector, Q (shown in Fig. 4). The scattering vector (Q) is defined in terms of scattering angles, θ, and wavelength, λ, of the radiation ($Q = 4\pi \sin\theta/\lambda$). The particle size distribution profile of Au NPs is shown in Fig. 4 inset. The average particle size was found to be ~27 nm.

3.2.5. X-ray photoelectron (XPS) analysis

XPS characterization of the GO nanosheets before and after deposition of the Au NPs was performed to understand the surface chemistry of the rGO nanosheets. This characterization also provides the information of reduction of the oxygen containing functional group and $AuCl^{4-}$ ions. GO nanosheets shows bands at 285 and 530 eV due to C1s and O1s, respectively (data not shown). It is described in our recent publication about the C1s XPS core level spectrum of GO nanosheets, and it can be deconvoluted into three components with binding energies at about 283.90, 285.90 and 287.81 eV assigned to C—C/C—H, C—O and C = O species, respectively [15]. This result indicates that the GO nanosheets contain large number of carboxyl, carbonyl, hydroxyl and epoxide functional groups. On the other hand, the C1s XPS core level spectrum of Au NPs-rGO composites is depicted in Fig. 5(a), and the peak at 284.47, 285.40, 286.60, 288.13 and 289.90 eV can be assigned to C=C, C—C, C—O, C=O and O—C=O, respectively. It is observed from the Fig. 5(a) that there is a decrease of the intensity of the peak of C—O, C = O and O—C=O compared to GO nanosheets, indicating the removal of oxygen containing functional groups of the Au NPs-rGO composites after reduction of the GO nanosheets in presence of Au NPs. The Au 4f spectrum was also detected and the binding energies of the Au $4f_{7/2}$ and Au $4f_{5/2}$ electrons of Au° are found to be at 82.2 and 85.8 eV (peak-to-peak distance 3.6 eV) conforms presence of Au° state particles (shown in Fig. 5(b)) [34].

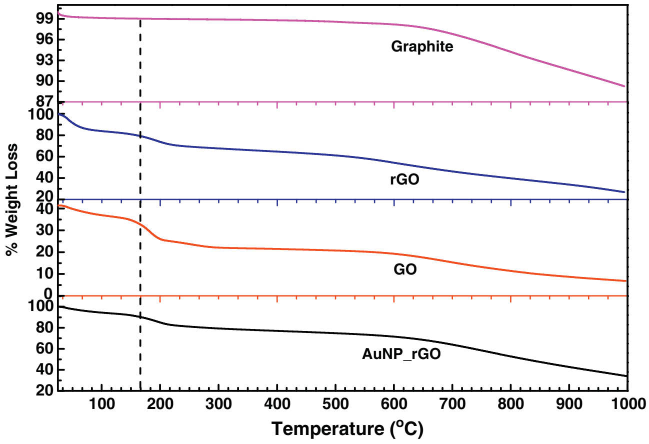

Fig. 2. TGA curve of graphite, rGO, GO and Au NPs-rGO composites.

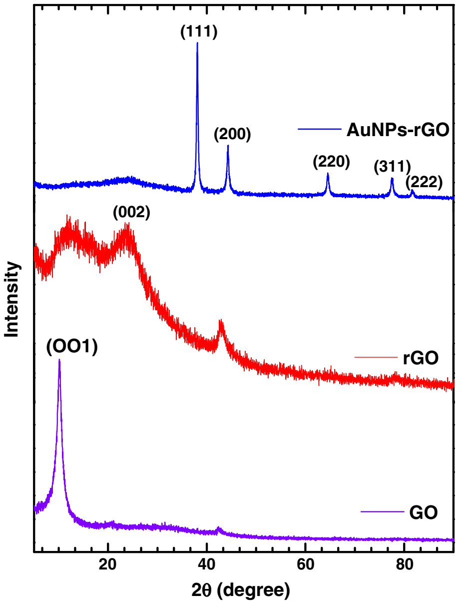

Fig. 3. Powder XRD diffractogram of GO, rGO and Au NPs-rGO composites.

3.2.6. Elemental analysis

The chemical constituents of GO, rGO and Au NPs-rGO composites were evaluated by CHN analysis (Table 1). It is observed from the Table 1 that the percentage of carbon and hydrogen content considerably increases upon formation of rGO which even increases more in case of Au NPs-rGO composites indicating better reduction of GO in presence of Au NPs [35].

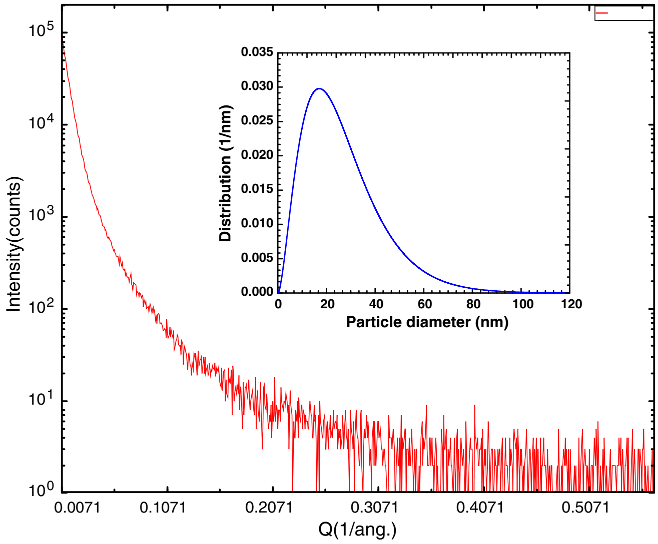

Fig. 4. SAXS curve of intensity against scattering vector (Q). Inset: particle size distribution profile of Au NPs on rGO nanosheets.

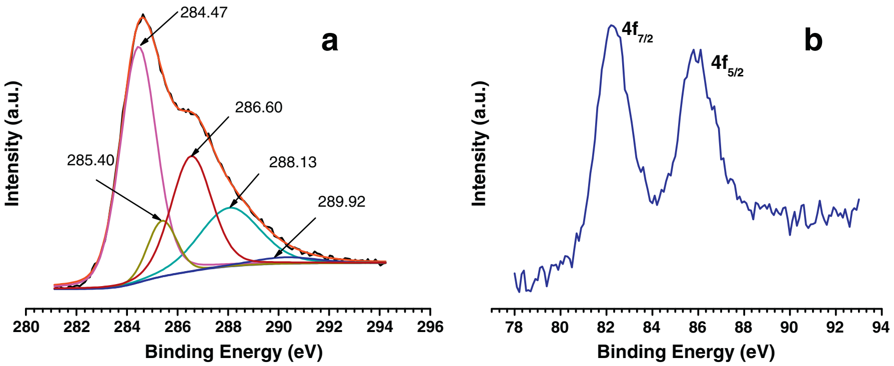

Fig. 5. XPS spectra of (a) C1s XPS spectra of AuNPs-rGO composites, and (b) Au4f core level XPS spectrum of AuNPs-rGO composites.

Table 1
CHN[*]analysis of GO, rGO and AuNP-rGO composites.

Materials	Elemental content (wt%)			C/O molar ratio
	C	H	O	
GO	44.00	2.96	53.02	1.11
rGO	65.46	0.93	33.54	2.60
Au NP_rGO composites	66.10	0.98	32.87	2.69

[*] As-received basis.

3.2.7. High resolution transmission electron microscope analysis

The morphology and structure of the Au NPs-rGO composites were investigated by high resolution transmission electron microscope (HRTEM). It is observed from Fig. 6a that the rGO nanosheets are non-uniformly folded, and Au NPs are distributed on that folded rGO sheets. Fig. 6(b–d) shows that a well-dispersed high density of Au NPs of the size range from 2 to 20 nm is deposited onto rGO nanosheets. The HRTEM images of Au NPs embedded on the rGO nanosheets are shown in Fig. 6e. The crystal lattice of the Au NPs and fringes of rGO nanosheets are resolved at few regions. The measured fringe lattice of Au NPs corresponds to the (111) plane is found to be 0.19 nm (Inset Fig. 6e). Fig. 6f shows that the diffraction dots are resolved in the selected area of electron diffraction (SAED) images, implying the crystalline nature of the Au NPs on the rGO nanosheets.

3.3. Catalytic application of Au NPs-rGO composites

The catalytic application of the synthesized Au NPs-rGO composites towards the oxidation of alcohol has been investigated. A variety of benzyl alcohols are smoothly oxidized to their corresponding aldehydes with high yields. During the reaction, other functional groups such as alkyl, methoxy and chloro remain intact (Table 2). The influence of the reaction conditions (viz. reaction time and temperature) on the process performance has also been studied and presented in Table 3. It is interesting to note that benzyl benzoate is the only side product formed. Benzoic acid is responsible for the formation of this side product, which is formed due to the over-oxidation of benzaldehyde. The

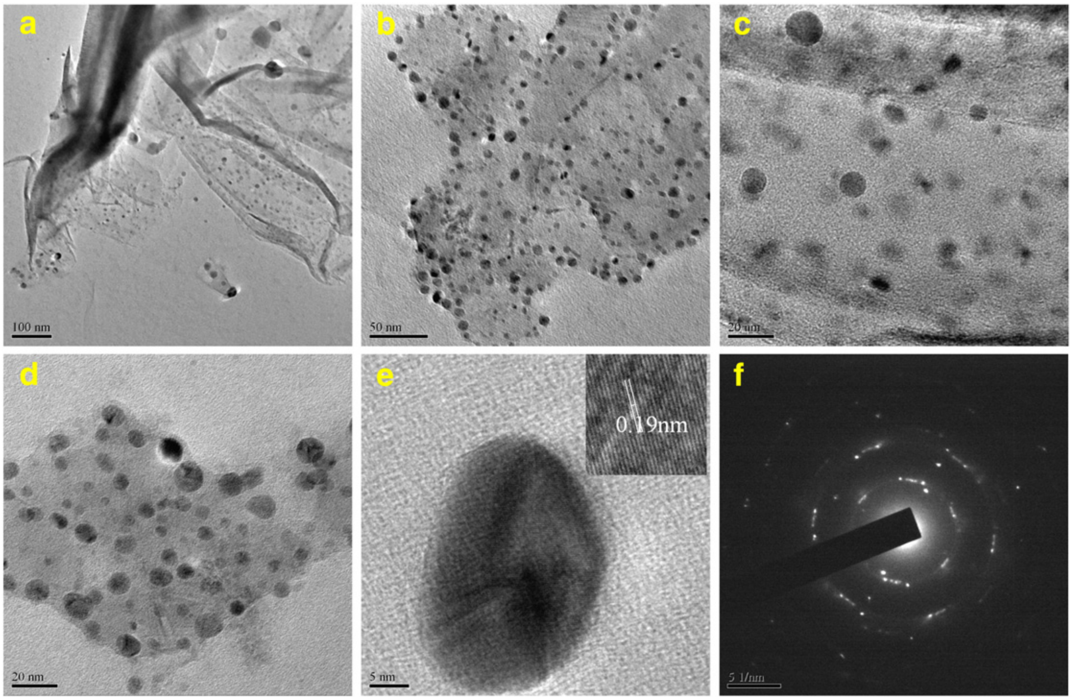

Fig. 6. TEM images of Au NPs on rGO nanosheets synthesized using 1 × 10^{-3} mol dm^{-3} $HAuCl_4$ solution by ascorbic acid reduction process under microwave irradiation: (a–d) TEM images, (e) HRTEM images along with fringe spacing (0.19 nm) in enlarged form, (f) SAED image of the Au NPs (1 × 10^{-3} mol dm^{-} $HAuCl_4$ solution).

Table 2
Au NPs-rGO-catalyzed the oxidation of benzyl alcohols to their corresponding carbonyls[a].

Entry	Substrate (1a–e)	Product (2a–e)[b]	Yield (%)[c]	TOF (h^{-1})[d]
1	PhCH$_2$OH (**1a**)	PhCHO (**2a**)	75	524.04
2	4-MeOPhCH$_2$OH (**1b**)	4-MeOPhCHO (**2b**)	77	531.01
3	4-MePhCH$_2$OH (**1c**)	4-MePhCHO (**2c**)	73	510.06
4	4-ClPhCH$_2$OH (**1d**)	4-ClPhCHO (**2d**)	67	468.14
5	3-NO$_2$PhCH$_2$OH (**1e**)	3-NO$_2$PhCHO (**2e**)	65	454.16

[a] Benzyl alcohol (1 mmol), aqueous suspension of Au-NP-rGO (2 mL), K$_2$CO$_3$ (4 mmol); the oxidation was carried out in an ACE pressure tube filled with oxygen at 130 °C.
[b] The products were characterized by comparison of physical and spectral data.
[c] Isolated yield.
[d] TOF: turn over frequency.

formation of this side product can be considerably lowered by reducing the reactive temperature and/or the reaction time. It was observed that with increase in reaction period and temperature, the benzyl alcohol conversion is increased. However, there is a small decrease in the selectivity for benzaldehyde due to the formation of benzyl benzoate. Results of the Au NPs-rGO composites catalyzed the oxidation of benzyl alcohols to their corresponding aldehydes are summarized in Table 2. The catalytic performance of the Au NPs-rGO is compared with earlier supported Au catalyst is presented in Table 4. Among all the reported catalyst, the Au NPs-rGO, using O$_2$ as the oxidizing agent, showed highest yield of benzaldehyde. TEM and SAXS investigation (shown in supplementary materials, Figs. S2 and S3) also shows that the morphology and size distribution of the Au NPs on the rGO nanosheets remain unchanged after the performance of the catalytic reaction.

Table 3
Effect of reaction conditions for the conversion of benzyl alcohol (**1a**) to benzaldehyde (**2a**)[a].

Entry	Reaction temperature (°C)	Reaction time (h)	Yield (%) of benzaldehyde	Yield of benzyl benzoate
1	90	7	30	ND
2	100	7	45	ND
3	110	5	60	Trace
4	120	3	70	Trace
5	120	4	70	Trace
6	**130**	**4**	**75**	**Trace**
7	130	5	72	10
8	140	4	68	18
9	160	4	66	26

ND: not detected.
[a] Benzyl alcohol, **1a** (1 mmol), aqueous suspension of Au-NP-rGO (2 mL), K$_2$CO$_3$ (4 mmol); the oxidation was carried out in an ACE pressure tube filled with oxygen.

Table 4
Comparison of the Au NPs-rGO catalyst for the oxidation of benzyl alcohol with earlier reported catalyst.

Catalyst	Oxidizing agent	Temperature (°C)	Time (h)	Yield (%)	Ref.
Au/U$_3$O$_8$	O$_2$	130	5	50	[26]
Au/MgO	TBHP	94	0.5	73	[27]
Au/MgO	O$_2$	130	5	44	[28]
Au-Pd/TiO$_2$	O$_2$	100	0.5	1.9	[29]
Au/TiO$_2$	TBHP	94	2.0	50	[30]
Au NPs-rGO	O$_2$	130	4	75	Present work

4. Conclusion

Au NPs-rGO composites were successfully synthesized using environment friendly reducing agent, ascorbic acid. The well-dispersed spherical Au NPs on rGO nanosheets have a size range of ~2-20 nm. The composites material show promising catalytic activity towards the halogen- and solvent-free oxidation of substituted benzyl alcohols by O$_2$ to their corresponding aldehydes with good selectivity and yields.

Acknowledgements

The authors thank the Department of Science and Technology, New Delhi, for financial support and also the Director, CSIR-North East Institute of Science and Technology, Jorhat, India, for the interest in this work. P. Sharma and P. Bezboruah are thankful to CSIR, New Delhi, and UGC, New Delhi, respectively, for senior research fellowship grant. The authors also acknowledge SAIF, NEHU, Shillong, for TEM images and Dr. K. R. Patil, Scientist, NCL, Pune for XPS analysis.

Appendix A. Supplementary data

Supplementary data to this article can be found online at http://dx.doi.org/10.1016/j.catcom.2013.06.021.

References

[1] K.S. Novoselov, A.K. Geim, S.V. Morozov, D. Jiang, Y. Zhang, S.V. Dubonos, I.V. Grigorieva, A.A. Firsov, Science 306 (2004) 666–669.
[2] A.K. Geim, K.S. Novoselov, Nature Materials 6 (2007) 183–191.
[3] K.S. Novoselov, A.K. Geim, S.V. Morozov, D. Jiang, M.I. Katsnelson, I.V. Grigorieva, S.V. Dubonos, A.A. Firsov, Nature 438 (2005) 197–200.
[4] X. Li, X. Wang, L. Zhang, S. Lee, H. Dai, Science 319 (2008) 1229–1232.
[5] S. Stankovich, D.A. Dikin, G.H.B. Dommett, K.M. Kohlhaas, E.J. Zinney, E.A. Stach, R.D. Piner, S.T. Nguyen, R.S. Ruoff, Nature 442 (2006) 282–286.
[6] F. Schedin, A.K. Geim, S.V. Morozov, E.W. Hill, P. Blake, M.I. Katsnelson, K. Novoselov, Nature Materials 6 (2007) 652–655.
[7] D. Li, M.B. Muller, S. Gilje, R.B. Kaner, G.G. Wallance, Nature Nanotechnology 3 (2008) 101–105.
[8] S. Park, R.S. Ruoff, Nature Nanotechnology 4 (2009) 217–224.
[9] Z.S. Pillai, P.V. Kamat, The Journal of Physical Chemistry. B 108 (2004) 945–951.
[10] C. Xu, X. Wang, J. Zhu, Journal of Physical Chemistry C 112 (2008) 19841–19845.
[11] Y. Sun, Y. Xia, Science 298 (2002) 2176–2179.
[12] G. Hodes, Advanced Materials 19 (2007) 639–655.
[13] J. Shen, M. Shi, N. Li, B. Yan, H. Ma, Y. Hu, M. Ye, Nano Research 3 (2010) 339–349.
[14] M.R. Das, R.K. Sarma, R. Saikia, V.S. Kale, M.V. Shelke, P. Sengupta, Colloids and Surfaces B: Biointerfaces 83 (2011) 16–22.
[15] M.R. Das, R.K. Sarma, S.C. Borah, R. Kumari, R. Saikia, V.S. Kale, A.B. Deshmukh, M.V. Shelke, P. Sengupta, S. Szunerits, R. Boukherroub, Colloids and Surfaces B: Biointerfaces 105 (2013) 128–136.
[16] R. Muszynski, B. Seger, P.V. Kamat, Journal of Physical Chemistry C 112 (2008) 5263–5266.
[17] H. Zhao, J. Yang, L. Wang, C. Tian, B. Jianga, H. Fu, Chemical Communications 47 (2011) 2014–2016.
[18] Y.G. Zhou, J.J. Chen, F.B. Wang, Z.H. Sheng, X.H. Xia, Chemical Communications 46 (2010) 5951–5953.
[19] K. Vinodgopal, B. Neppolian, I.V. Lightcap, F. Grieser, M. Ashokkumar, P.V. Kamat, Journal of Physical Chemistry Letters 1 (2010) 1987–1993.
[20] P. Kundu, C. Nethravathi, P.A. Deshpande, M. Rajamathi, G. Madras, N. Ravishankar, Chemistry of Materials 23 (2011) 2772–2780.
[21] J.L. Kroschwitz, 4th ed., Encyclopedia of Chemical Technology, vol. 4, Wiley-Interscience Publications, New York, 1992.
[22] R. Sumathi, K. Johnson, B. Vishwanthan, T.K. Varadarajan, Applied Catalysis A: General 172 (1998) 15–22, (References cited therein).
[23] L.F. Liotta, A.M. Venezia, G. Deganello, A. Longo, A. Martorana, Z. Schay, L. Guczi, Catalysis Today 66 (2001) 271–276.
[24] G.D. Yadav, C.K. Mistry, Journal of Molecular Catalysis A: Chemical 172 (2001) 135–149.
[25] B.M. Choudary, M.L. Kantam, A. Rahman, C.V. Reddy, K.K. Rao, Angewandte Chemie (International Ed. in English) 40 (2001) 763–766.
[26] V.R. Choudhary, R. Jha, P. Jana, Green Chemistry 9 (2007) 267–272.
[27] V.R. Choudhary, D.K. Dumbre, Catalysis Communications 10 (2009) 1738–1742.
[28] V.R. Choudhary, A. Dhar, P. Jana, R. Zha, B.S. Uphade, Green Chemistry 7 (2005) 768–770.
[29] D.I. Enache, D. Barker, J.K. Edwards, S.H. Taylor, D.W. Knight, A.F. Carley, G.J. Hutchings, Catalysis Today 122 (2007) 407–411.

[30] D.I. Enache, J.K. Edwards, P. London, B. Sulsana-Espriu, A.F. Carley, A.A. Herzing, M. Watanabe, C.J. Kiely, D.W. Knight, G.J. Hutchings, Science 311 (2006) 362–365.
[31] A. Villa, D. Wang, N. Dimitratos, D. Su, V. Trevisan, L. Prati, Catalysis Today 150 (2010) 8–15.
[32] A. Abad, P. Concepcion, A. Corma, H. Garcia, Angewandte Chemie International Edition 44 (2005) 4066–4069.
[33] W.S. Hummer, R.E. Offeman, Journal of the American Chemical Society 80 (1958) 1339.
[34] F. Li, H. Yang, C. Shan, Q. Zhang, D. Han, A. Ivaska, L. Niu, Journal of Materials Chemistry 19 (2009) 4022–4025.
[35] W. Yue, S. Jiang, W. Huang, Z. Gao, J. Li, Y. Ren, X. Zhao, X. Yang, Journal of Materials Chemistry A 1 (2013) 6928–6933.